Available online at www.sciencedirect.com
SCIENCE DIRECT
Journal of volcanology and geothermal research
ELSEVIER
Journal of Volcanology and Geothermal Research 152 (2006) 1–19
www.elsevier.com/locate/jvolgeores

The evolution of a chemically zoned magma chamber: The 1707 eruption of Fuji volcano, Japan

S. Watanabe [a,*], E. Widom [a], T. Ui [b,1], N. Miyaji [c], A.M. Roberts [a]

[a] *Department of Geology, Miami University, Oxford, OH 45056, USA*
[b] *Department of Earth and Planetary Sciences, Hokkaido University, Sapporo 060-0810, Japan*
[c] *Department of Geosystem Sciences, Nihon University, Tokyo 156-8550, Japan*

Received 8 June 2004; received in revised form 12 August 2005; accepted 29 August 2005
Available online 14 November 2005

Abstract

The eruptive history of Fuji volcano has been dominated by basaltic volcanism. However, the 1707 eruption of Fuji volcano resulted in a chemically zoned pyroclastic deposit ranging from basalt to dacite. The processes responsible for generating these silicic magmas at Fuji volcano are not well understood, although it has been proposed that liquid immiscibility played a major role. In order to further constrain the petrogenetic processes that occurred prior to the 1707 eruption, detailed petrographic, major and trace element, and Sr, Nd, Pb, and Os isotope studies were done. A comprehensive suite of samples spans a wide range of SiO_2 from 50 to 67 wt.% (basalt to dacite); however, there is a compositional gap between 52 and 57 wt.% SiO_2. Least squares major element modeling can explain the observed major element variations with fractionation of the observed mineral phases and low sum of squares of residuals (0.07–0.31). The results of trace element modeling using literature-derived mineral–liquid Kd values are consistent with the major element modeling. Sr, Nd, and Pb isotopes show essentially identical signatures throughout the deposit with $^{87}Sr/^{86}Sr = 0.70340 \pm 1$, $^{143}Nd/^{144}Nd = 0.51304 \pm 1$, $^{206}Pb/^{204}Pb = 18.25 \pm 2$, $^{207}Pb/^{204}Pb = 15.48 \pm 1$, and $^{208}Pb/^{204}Pb = 38.16 \pm 3$. These results are consistent with closed-system fractionation. However, open-system behavior is indicated by Os isotopes. The $^{187}Os/^{188}Os$ isotopes of the andesite and dacites (0.26–0.39) are distinctly more radiogenic than the basalts (0.165–0.174). These radiogenic signatures can be explained by ≤0.2% crustal assimilation, which would not significantly affect the Sr, Nd, or Pb isotope signatures. Disequilibrium textures in plagioclase crystals are also consistent with open-system behavior. The petrographic, geochemical, and isotopic observations suggest that the 1707 chemically zoned magma chamber of Fuji volcano evolved through three main stages including fractionation of a parental basaltic magma, formation of an evolved chemically zoned magma chamber via fractional crystallization and minor crustal assimilation, and basaltic intrusion into the magma chamber, which may have triggered the 1707 AD eruption.

Keywords: Fuji volcano; magma chamber; isotope geochemistry; fractional crystallization

1. Introduction

Many deposits from large, explosive volcanic eruptions are chemically zoned, representing chemical gradients in the magma chamber feeding the volcano. Magma generally becomes more silicic and volatile-rich towards the top of the chamber as it evolves,

* Corresponding author. Tel.: +1 513 529 3227; fax: +1 513 529 1542.
E-mail address: watanas@muohio.edu (S. Watanabe).
[1] Present address: Crisis and Environment Management Policy Institute, Kansai Office, 3-7-4 Chigusa, Takarazuka, 665-0072, Japan.

0377-0273/$ - see front matter © 2005 Elsevier B.V. All rights reserved.
doi:10.1016/j.jvolgeores.2005.08.002

becoming potentially explosive. Closed-system crystal fractionation can often produce such complex magma chambers (Michael, 1983; Wörner and Schmincke, 1984; Widom et al., 1992), and several recent detailed geochemical and isotopic studies have revealed the importance of open-system processes such as magma mixing and crustal assimilation in some cases (Wörner and Wright, 1984; Duffield et al., 1995; Wolff and Ramos, 2003; Snyder et al., 2004).

The most recent eruption of Fuji volcano, in 1707 AD, resulted in a chemically zoned volcanic deposit ranging from basalt to dacite (Tsuya, 1955). Such silicic eruptions have occurred only twice in the history of Fuji Volcano, in 2800 BP and in 1707 AD; most eruptions throughout Fuji's history have been dominated by basalt (Miyaji, 1988). Despite the unusual nature of the 1707 eruption, little work has been done to unravel the processes that led to the silicic, chemically zoned deposit. Kawamoto (1990, 1991a,b, 1992) proposed that liquid immiscibility was an important process in generating a chemically zoned magma chamber prior to the 1707 eruption. Evidence for liquid immiscibility has been found in some mafic magmas such as high-alumina and tholeiitic basaltic magmas (Philpotts, 1976, 1982; Fujii et al., 1980) and in some olivine basalts from older eruptions of Fuji volcano, which contain Fe-rich silicate globules that are up to 10 μm (Fujii et al., 1980). However, apart from possible generation of carbonatite magmas (Brooker, 1998), liquid immiscibility has not previously been recognized as a process that could produce magma chamber-scale chemical gradients or silicic magmas such as andesite and dacite.

The purpose of this study was to carefully evaluate the role of potential petrogenetic processes including fractional crystallization, magma mixing, crustal assimilation, and liquid immiscibility, in the development of the chemically zoned 1707 deposit of Fuji volcano. This is the first study to combine petrographic, major and trace element, and Sr, Nd, Pb, and Os isotope data to develop a detailed petrogenetic model of the evolution of the Fuji 1707 magmatic system.

2. Geological setting/background

Fuji volcano is located in south-central Honshu, Japan; it lies over the westward subducting Pacific plate and may be influenced by the Philippine Sea plate (Arculus et al, 1991; Fig. 1). The main edifice of Fuji volcano consists of three volcanoes including Komitake, Older Fuji, and Younger Fuji (oldest to youngest, respectively; Tsuya, 1940). The oldest known deposits from Fuji were formed approximately 80,000 yr ago (Machida, 1964). Fuji volcano has been very active throughout its history and erupted predominantly medium K series high-alumina basalts with SiO_2 ranging from 48 to 52 wt.% (Togashi, 1990; Arculus et al, 1991). Sr and Nd isotope signatures in Fuji eruptive products display a narrow range with $^{87}Sr/^{86}Sr$ varying from 0.70335 to 0.70355 and $^{143}Nd/^{144}Nd$ varying from 0.51300 to 0.51305 (Togashi, 1990). These values fall within the range of typical Izu-Bonin arc basalts ($^{87}Sr/^{86}Sr$=~0.7029–0.7040, $^{143}Nd/^{144}Nd$=~0.5130–0.5131; Taylor and Nesbitt, 1998; Hochstaedter et al., 2001), but are less radiogenic than most other basalts from Japan ($^{87}Sr/^{86}Sr$=~0.7030–0.7075, $^{143}Nd/^{144}Nd$=~0.5125–0.5131; Honda and Wasserburg, 1981; Ishizuka and Carlson, 1983; Kimura et al., 1999; Hoang and Uto, 2003).

The most recent eruption in 1707 AD was the most explosive eruption in the history of Fuji volcano and resulted in a chemically zoned volcanic deposit ranging from basalt to dacite. The Plinian eruptions that produced the dacitic and andesitic pumices began in the morning of December 16, 1707, and lasted until that evening. Soon after the end of the silicic eruptions, a much greater volume subplinian to Plinian basaltic eruption began and lasted until January 1, 1708 (Koyama et al., 2002). These eruptions formed three craters on the SE flank of the volcano, which are called Hoei first, second, and third craters from the top to the bottom (Fig. 1). Silicic eruptions took place at the second and third craters, and the later basaltic eruption took place at the first crater (Tsuya, 1955). These craters are aligned in a NW–SE direction, coinciding with the Philippine Sea plate's main axis of compression. The 1707 deposit has previously been subdivided into four units, Ho I to Ho IV from the bottom to the top, based on differences in grain size and constituents (Miyaji, 1984). Ho I contains both dacitic and andesitic pumices. Ho II contains only andesitic pumice. Ho III and Ho IV consist of basaltic scoria with variable vesicularity that increases from Ho III to Ho IV. The total eruptive volume was 0.7 km^3 (Miyaji, 1984).

3. Analytical techniques

A comprehensive suite of samples for this study was collected from two localities. The first sampling locality (Taroubou) is ~5 km SE of the craters (35°19′883″N, 138°47′831″E) and exhibits an incomplete eruption record with an absence of Ho III and Ho IV, but greater thicknesses of Ho I (22 cm) and Ho II (100 cm). The second sampling site, ~4 km NE of the craters (35°21′703″N, 138°47′831″E), displays a complete de-

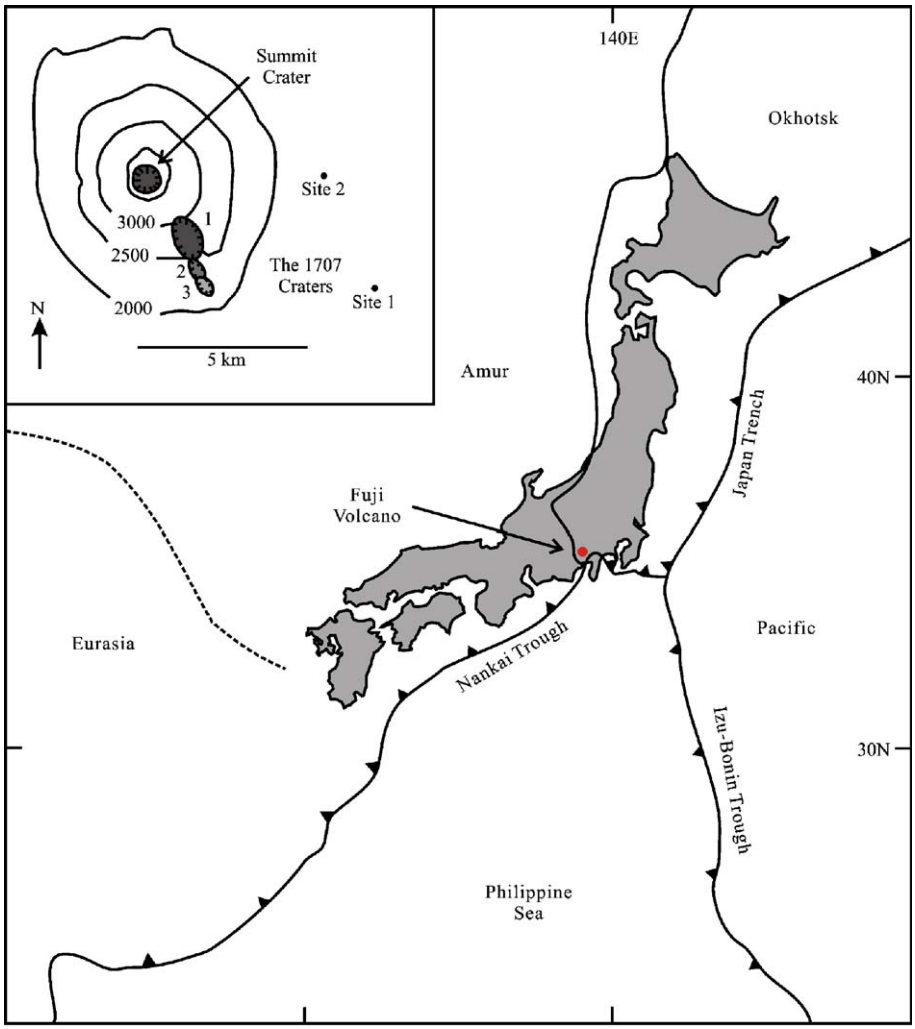

Fig. 1. Plate tectonic framework of Japan (modified after Taira, 2001). The inset is a cartoon diagram of the three craters formed during the 1707 eruption (modified after Koyama, 1998), with the locations of sampling sites 1 and 2.

positional section of the 1707 eruption (Fig. 2). The thicknesses of the representative units at this site are 18, 19, 115, and 125 cm, respectively.

Major and trace element concentrations of whole rocks were obtained by DCP-AES (Direct-Current Plasma Atomic Emission Spectrometry) at Miami University. For the rare-earth element (REE) measurements, bulk REE separations were done by ion exchange with AG50W-X8 cation-exchange resin, followed by clean-up columns with AG50W-X12 resin. Sample preparation and measurement methods are described in Katoh et al. (1999). Mineral chemistry was obtained by electron microprobe analysis (Cameca SX 50) at Indiana University, Bloomington, IN.

Chemical separations and Sr, Nd, Pb, and Os isotopic measurements were done at Miami University. For Sr, Nd, and Pb analyses, approximately 0.1 g of whole rock powder was dissolved in concentrated HF–HNO_3 and taken up in HBr. Procedures for the Sr, Pb, and bulk rare earth separations are described in Walker et al. (1989) and Snyder (2005). EiChrom Ln-Spec resin was used for Sm–Nd separations following methods similar to Pin and Zalduegui (1997).

Sample digestion for Re–Os chemistry followed the Carius tube method described in Shirey and Walker (1995). Separation of Re and Os were done using an aqua regia–CCl_4 solvent extraction technique (Cohen and Waters, 1996), and back-extracted into HBr. Samples were then further purified using a microdistillation procedure (Roy-Barman, 1993; Roy-Barman and Allegre, 1995).

All isotopic compositions were measured by thermal ionization mass spectrometry using a Finnigan Triton. Strontium isotopic ratios were corrected for mass frac-

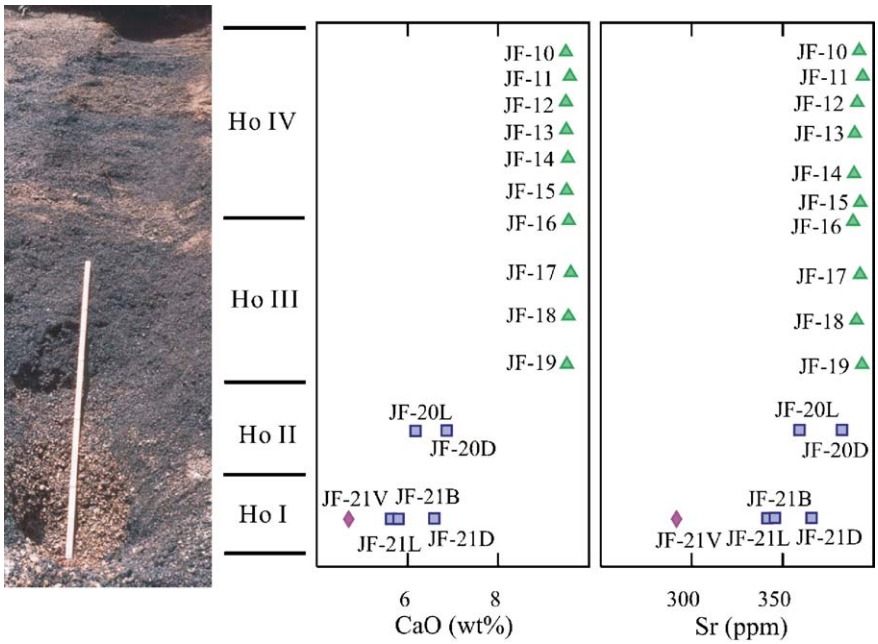

Fig. 2. A photograph of the second sampling site and the variation in CaO (wt.%) and Sr concentration (ppm) with depth. The vertical axis is Miyaji's (1984) stratigraphy. The total thickness of the deposit is 277 cm. Triangles, squares, and diamonds represent basalt, andesite, and dacite, respectively.

tionation using $^{86}Sr/^{88}Sr=0.1194$. Sixty-eight measurements of NBS 987 gave an average of $^{87}Sr/^{86}Sr=0.710236\pm0.000014$ (2 S.D.). Neodymium isotopic ratios were corrected for mass fractionation using $^{144}Nd/^{146}Nd=0.7219$. Sixty-one measurements of La Jolla gave an average of $^{143}Nd/^{144}Nd=0.511846\pm0.000007$ (2 S.D.). $^{206}Pb/^{204}Pb$, $^{207}Pb/^{204}Pb$, and $^{208}Pb/^{204}Pb$ were corrected for fractionation by 0.11% per amu, based on deviations of measured ratios in NBS 981 from values in Todt et al. (1996). Errors on $^{206}Pb/^{204}Pb$, $^{207}Pb/^{204}Pb$, and $^{208}Pb/^{204}Pb$ (2 S.D.) based on 58 measurements of NBS 981 were ±0.01, ±0.02, and ±0.06, respectively. Osmium was measured by negative thermal ionization as OsO_3^-. Osmium isotope ratios were corrected for oxygen using the oxygen isotopic abundances of Nier (1950) and for mass fractionation using $^{192}Os/^{188}Os=3.0826$. Internal measurement errors for osmium isotopic ratios ranged from 0.5% to 2%. Blank correction errors ranged from 0.6% to 10% based on blanks of 1.0 ± 0.1 pg and $^{187}Os/^{188}Os=0.174$. Replicate analyses (JF-15 and JF-15R) agreed within 3.6% for $^{187}Os/^{188}Os$.

4. Results

Chemical compositions of 37 juvenile and 12 lithic fragment samples were analyzed using DCP-AES (Table 1). JF-20 and JF-21 are heterogeneous with mixture of pumices and scorias. In order to get meaningful whole rock chemistry, JF-20 was separated into dark (JF-20D) and light (JF-20L) fractions, while JF-21 was separated into dark (JF-21D), light (JF-21L), very light (JF-21V), and banded (JF-21B) fractions. All juvenile samples are subalkaline medium-K basalt, andesite, and dacite, respectively (Fig. 3).

4.1. Major elements

The juvenile samples from the 1707 deposit show substantial major element variations. SiO_2 ranges from 50 to 67 wt.% (basalt to dacite); however, there is a compositional gap between 52 and 57 wt.% (Table 1). TiO_2, Al_2O_3, Fe_2O_3, MnO, MgO, CaO, and P_2O_5 decrease with increasing SiO_2, while Na_2O and K_2O increase with increasing SiO_2. Elemental abundances show variations with relative depth in the deposit (Fig. 2). The deposit generally becomes more mafic from the bottom to the top, although as noted above, some samples from individual stratigraphic horizons are heterogeneous.

4.2. Trace elements

Trace elements analyzed by DCP-AES include Ni, Zn, Cu, Cr, Zr, V, Sc, Ba, Sr, Rb, and Y (Table 1). All

Table 1
Major and trace element concentrations of juvenile and lithic samples from the 1707 Fuji deposit. Major elements are in weight percent. Trace elements are in parts per million

Sampling site 1														
Sample units	JF-2a Ho II	JF-2b Ho II	F-2c Ho II	JF-2d Ho II	JF-2e Ho II	JF-2f Ho II	JF-3a Ho II	JF-3b Ho II	JF-3c Ho II	JF-3d Ho II	JF-3e Ho II	JF-3f Ho II	JF-4a Ho II	JF-4b Ho II
SiO_2	58.14	57.25	57.04	59.83	57.80	64.05	61.47	60.63	62.05	59.84	59.82	63.48	59.47	59.67
TiO_2	1.13	1.07	1.10	0.96	1.07	0.83	0.91	1.01	0.90	1.03	0.99	0.82	1.03	1.01
Al_2O_3	16.80	16.29	16.57	15.93	16.49	15.92	15.87	16.34	16.05	16.37	16.19	15.79	16.40	16.42
Fe_2O_3	8.88	8.33	8.53	7.42	8.35	6.12	6.93	7.91	6.72	8.04	7.58	6.23	8.20	7.74
MnO	0.17	0.16	0.17	0.15	0.16	0.13	0.14	0.15	0.13	0.16	0.15	0.13	0.16	0.15
MgO	3.17	2.94	3.03	2.48	2.95	1.89	2.25	2.67	2.19	2.73	2.54	1.97	2.87	2.62
CaO	6.79	6.40	6.58	5.80	6.37	5.07	5.42	6.12	5.34	6.31	5.88	5.10	6.46	5.99
Na_2O	3.61	3.55	3.58	3.64	3.56	3.77	3.65	3.64	3.68	3.66	3.64	3.75	3.66	3.64
K_2O	1.39	1.40	1.36	1.60	1.41	2.10	1.80	1.65	1.88	1.59	1.59	2.14	1.51	1.57
P_2O_5	0.33	0.35	0.35	0.29	0.31	0.25	0.29	0.31	0.28	0.29	0.29	0.25	0.32	0.32
LOI	−0.03	−0.08	−0.12	0.05	0.02	0.23	0.02	0.00	0.23	−0.11	−0.03	0.23	−0.01	0.05
Total	100.39	97.67	98.18	98.13	98.50	100.35	98.74	100.44	99.45	99.90	98.63	99.89	100.06	99.19
Ni	12	8	0	7	13	5	5	7	4	7	1	11	14	5
Zn	102	111	108	86	87	85	79	100	86	89	88	83	101	95
Cu	69	68	74	69	71	57	65	70	61	71	74	54	76	74
Cr	0	6	3	0	9	0	7	1	5	0	2	0	2	2
Zr	142	145	137	145	138	166	154	151	153	148	147	166	140	145
V	207	193	193	180	205	124	166	184	141	185	184	136	185	183
Sc	23	24	24	19	23	15	19	21	18	21	21	16	22	23
Ba	375	368	360	403	364	–	422	401	404	397	395	495	386	392
Sr	391	364	374	341	367	316	325	362	322	370	347	316	373	354
Rb	34	21	24	47	46	53	38	24	35	40	32	43	24	41
Y	35	34	33	32	33	32	34	34	33	33	33	34	34	33
La	12.1	–	–	–	–	–	–	12.9	–	–	–	13.0	–	–
Ce	33.5	–	–	–	–	–	–	35.4	–	–	–	36.0	–	–
Nd	20.8	–	–	–	–	–	–	21.5	–	–	–	21.0	–	–
Sm	5.4	–	–	–	–	–	–	5.5	–	–	–	5.4	–	–
Eu	1.6	–	–	–	–	–	–	1.5	–	–	–	1.3	–	–
Gd	6.0	–	–	–	–	–	–	5.8	–	–	–	5.6	–	–
Dy	5.5	–	–	–	–	–	–	5.8	–	–	–	5.5	–	–
Er	3.4	–	–	–	–	–	–	3.4	–	–	–	3.3	–	–
Yb	3.3	–	–	–	–	–	–	3.5	–	–	–	3.4	–	–
Lu	0.5	–	–	–	–	–	–	0.5	–	–	–	0.5	–	–

	Sampling site 1							Sampling site 2					
	JF-4d Ho II	JF-4e Ho II	JF-4f Ho II	JF-5a Ho I	JF-5b Ho I	JF-5c Ho I	JF-5d Ho I	JF-10 Ho IV	JF-11 Ho IV	JF-12 Ho IV	JF-13 Ho IV	JF-14 Ho IV	JF-15 Ho IV
SiO_2	60.62	64.55	62.71	62.73	61.90	66.51	66.75	50.41	51.43	50.50	50.78	50.61	51.61
TiO_2	0.98	0.77	0.83	0.88	0.92	0.68	0.69	1.35	1.36	1.35	1.34	1.33	1.34
Al_2O_3	16.17	15.46	15.76	15.77	16.04	15.14	15.26	17.06	17.11	16.80	16.76	17.14	17.10
Fe_2O_3	7.46	5.69	6.35	6.67	6.82	4.87	4.84	11.92	11.87	11.98	11.96	11.90	11.84
MnO	0.14	0.12	0.13	0.14	0.13	0.11	0.10	0.19	0.19	0.19	0.19	0.19	0.19
MgO	2.48	1.76	1.98	2.11	2.16	1.43	1.41	5.26	5.23	5.30	5.28	5.30	5.26
CaO	5.82	4.76	5.19	5.50	5.41	4.26	4.13	9.59	9.60	9.59	9.51	9.51	9.49
Na_2O	3.66	3.75	3.80	3.79	3.70	3.81	3.71	2.70	2.68	2.63	2.62	2.65	2.83
K_2O	1.64	2.27	2.06	1.94	1.78	2.52	2.41	0.73	0.74	0.73	0.72	0.93	0.67
P_2O_5	0.32	0.21	0.27	0.28	0.28	0.21	0.19	0.23	0.26	0.23	0.35	0.25	0.22
LOI	0.01	0.53	0.34	−0.06	−0.01	0.31	0.35	−0.21	−0.27	−0.18	−0.24	−0.26	−0.23
Total	99.29	99.88	99.41	99.73	99.13	99.85	99.85	99.22	100.21	99.10	99.27	99.54	100.33
Ni	3	3	6	4	1	5	0	26	24	32	24	29	22
Zn	85	66	67	76	96	63	60	101	110	100	105	112	93
Cu	74	51	60	61	75	42	52	164	169	179	175	176	168

(continued on next page)

Table 1 (*continued*)

Sampling site 1								Sampling site 2					
	JF-4d Ho II	JF-4e Ho II	JF-4f Ho II	JF-5a Ho I	JF-5b Ho I	JF-5c Ho I	JF-5d Ho I	JF-10 Ho IV	JF-11 Ho IV	JF-12 Ho IV	JF-13 Ho IV	JF-14 Ho IV	JF-15 Ho IV
Cr	1	1	0	2	5	3	8	40	39	39	41	48	43
Zr	151	166	158	161	159	164	178	75	79	77	76	78	73
V	169	139	132	157	158	101	101	395	403	429	399	426	406
Sc	22	13	16	16	21	11	16	36	38	39	38	40	37
Ba	404	449	430	423	436	448	472	197	219	213	218	214	210
Sr	345	298	320	332	329	273	265	389	394	387	384	385	391
Rb	45	50	35	52	28	43	45	8	22	0	28	0	2
Y	35	33	33	32	35	29	36	23	26	26	26	26	24
La	–	–	–	–	–	14.1	–	7.0	–	–	–	–	6.1
Ce	–	–	–	–	–	37.9	–	18.9	–	–	–	–	15.7
Nd	–	–	–	–	–	21.9	–	13.5	–	–	–	–	11.9
Sm	–	–	–	–	–	5.5	–	3.8	–	–	–	–	3.5
Eu	–	–	–	–	–	1.2	–	1.2	–	–	–	–	1.1
Gd	–	–	–	–	–	5.7	–	4.0	–	–	–	–	3.1
Dy	–	–	–	–	–	6.0	–	4.2	–	–	–	–	4.1
Er	–	–	–	–	–	3.5	–	2.2	–	–	–	–	1.9
Yb	–	–	–	–	–	3.6	–	2.3	–	–	–	–	2.1
Lu	–	–	–	–	–	0.5	–	0.3	–	–	–	–	0.3

Sampling site 2										
	JF-16 Ho IV	JF-17 Ho III	JF-18 Ho III	JF-19 Ho III	JF-20L Ho II	JF-20D Ho II	JF-21V Ho I	JF-21L Ho I	JF-21D Ho I	JF-21B Ho I
SiO_2	50.96	51.01	50.87	51.52	60.43	58.43	65.26	62.37	59.48	61.96
TiO_2	1.33	1.34	1.33	1.33	1.03	1.12	0.75	0.94	1.04	0.95
Al_2O_3	16.89	17.14	16.93	17.16	16.47	16.61	15.47	16.21	16.41	16.20
Fe_2O_3	11.91	11.91	11.76	11.59	7.80	8.72	5.61	7.02	8.11	7.13
MnO	0.19	0.19	0.19	0.19	0.15	0.17	0.12	0.14	0.16	0.14
MgO	5.36	5.37	5.26	5.12	2.64	3.09	1.71	2.26	2.82	2.31
CaO	9.63	9.76	9.67	9.54	6.10	6.76	4.69	5.66	6.42	5.70
Na_2O	2.61	2.65	2.67	2.79	3.67	3.55	3.75	3.87	3.60	3.74
K_2O	0.72	0.72	0.73	0.80	1.61	1.30	2.29	1.77	1.44	1.78
P_2O_5	0.25	0.23	0.25	0.24	0.30	0.32	0.23	0.28	0.30	0.29
LOI	−0.23	−0.20	−0.29	−0.22	0.15	−0.03	0.39	0.10	−0.01	0.13
Total	99.63	100.12	99.38	100.05	100.37	100.05	100.28	100.06	99.76	100.33
Ni	26	19	21	19	9	12	4	5	10	5
Zn	89	104	108	86	92	99	71	95	90	105
Cu	174	178	171	161	75	81	54	69	79	66
Cr	43	42	42	38	5	8	0	0	1	0
Zr	73	76	73	80	145	131	172	152	137	148
V	396	375	423	371	176	198	109	143	186	155
Sc	36	36	39	36	21	24	14	19	22	18
Ba	219	214	213	231	383	364	461	406	371	410
Sr	386	392	389	393	363	383	292	342	365	345
Rb	7	0	19	11	51	37	45	51	28	34
Y	25	24	24	26	31	31	34	33	31	33

Lithics: basalt							Lithics: gabbro				
	JF-6a	JF-6b	JF-6c	JF-6d	JF-7a	JF-8a	JF-9b	JF-1	JF-4c	JF-7b	JF-8b	JF-9a
SiO_2	49.68	51.42	51.10	51.15	50.49	50.08	50.92	48.40	44.90	46.68	46.80	46.94
TiO_2	1.37	0.98	1.37	0.96	1.31	1.34	0.92	1.11	0.19	0.23	1.14	0.57
Al_2O_3	16.89	18.65	17.14	18.43	17.04	16.92	17.72	16.35	23.19	23.17	18.97	25.92
Fe_2O_3	12.60	10.18	12.16	10.67	11.80	12.25	10.52	12.14	7.67	6.24	12.70	5.65
MnO	0.19	0.15	0.19	0.17	0.18	0.19	0.17	0.18	0.12	0.10	0.16	0.08
MgO	5.94	5.51	5.06	5.43	6.33	6.14	6.10	7.81	8.82	7.60	7.69	2.81
CaO	9.87	9.37	9.40	9.60	9.80	9.99	10.28	10.23	13.29	14.74	11.44	14.64

Table 1 (*continued*)

	Lithics: basalt							Lithics: gabbro				
	JF-6a	JF-6b	JF-6c	JF-6d	JF-7a	JF-8a	JF-9b	JF-1	JF-4c	JF-7b	JF-8b	JF-9a
Na_2O	2.37	2.85	2.91	2.80	2.51	2.40	2.56	2.22	1.00	0.95	1.75	1.77
K_2O	0.60	0.51	0.68	0.47	0.59	0.54	0.37	0.13	0.05	0.03	0.18	0.09
P_2O_5	0.26	0.24	0.31	0.12	0.28	0.24	0.29	0.21	0.12	0.10	0.13	0.12
LOI	−0.39	−0.28	−0.30	−0.30	−0.29	−0.28	−0.11	−0.34	−0.27	−0.12	−0.35	−0.07
Total	99.39	99.60	100.02	99.50	100.05	99.79	99.73	98.45	99.08	99.72	100.61	98.51
Ni	49	48	26	25	57	36	38	64	83	77	64	13
Zn	102	82	119	90	98	107	95	102	133	36	89	45
Cu	199	114	147	84	170	196	94	40	15	12	64	53
Cr	57	55	30	31	110	99	81	110	153	276	137	84
Zr	71	48	71	39	76	71	41	13	6	8	22	5
V	409	314	385	367	386	399	336	461	64	100	459	220
Sc	38	32	32	31	41	43	35	41	19	28	36	17
Ba	205	160	208	150	196	202	133	81	37	39	81	73
Sr	363	397	410	396	363	354	359	382	463	452	419	590
Rb	5	17	13	10	11	18	5	0	3	14	35	7
Y	25	18	26	18	27	27	17	14	6	7	13	6

trace elements vary in concentration throughout the deposit. Ni, Zn, Cu, Cr, V, Sc, and Sr decrease with increasing SiO_2, while Zr, Ba, Rb, and Y increase with increasing SiO_2. Trace element concentration variations range in magnitude from <3-fold (Zn, Zr, Ba, Y, Sr) to >5-fold (Ni, Cr, Rb). Intermediate (3–5 fold) variations are observed for Cu, V, and Sc.

REE abundances increase from basalt to andesite. There is a slight increase in light REE (LREE) and no increase in middle REE (MREE) and heavy REE (HREE) from andesite to least evolved dacite and from the least evolved to most evolved dacite (Table 1; Fig. 4A). Negative Eu anomalies are absent in the basalts, but increase in magnitude from andesite to most evolved dacite.

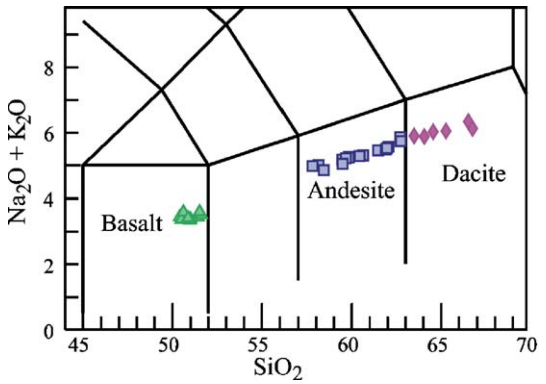

Fig. 3. Alkali vs. silica classification diagram (after LeBas et al., 1986). The samples span a wide range of SiO_2 from 50 to 67 wt % (basalt to dacite); however, there is a compositional gap between 52 and 57 wt.% SiO_2.

4.3. Petrography and mineral chemistry

4.3.1. Juvenile rocks

Juvenile fragments in the 1707 deposit include basalt, andesite, and dacite, in decreasing abundance. They are all vesicular and vitrophyric. From the least evolved to most evolved samples, the amount of glassy matrix increases and the percentage of phenocrysts decreases from ~10 to ~2 vol.% (basalt to dacite). Predominant mineral phases in the 1707 deposit include plagioclase, olivine, hypersthene, augite, magnetite, and apatite. Plagioclase is the most abundant phenocryst phase throughout the deposit and ranges in size from microphenocrysts (<0.5 mm) to 2 mm. Mineral chemistry of representative samples was obtained by electron microprobe and average values are summarized in Table 2. Feldspar chemical compositions are shown in Fig. 5. Small fragments of gabbroic xenocrysts are sometimes present in silicic pumices and scoria in Ho III.

Basalt is the most abundant rock type. Predominant mineral phases in the basalt are plagioclase, olivine, augite, and magnetite. The core of plagioclase phenocrysts in the basalt have anorthite values of $An_{70–80}$ and show normal zoning. Some plagioclase crystals show evidence of disequilibrium including resorbed and sieved textures. The cores of those crystals show a wider range in compositions ($An_{70–90}$). Mg-rich olivine ($Fo_{70–79}$) is present only in the basalt, and some are resorbed. The matrix consists of dark black non-vesicular regions intermingled with a slightly lighter highly vesicular matrix. In general, the former matrix contains a wider range of phenocryst sizes (0.5

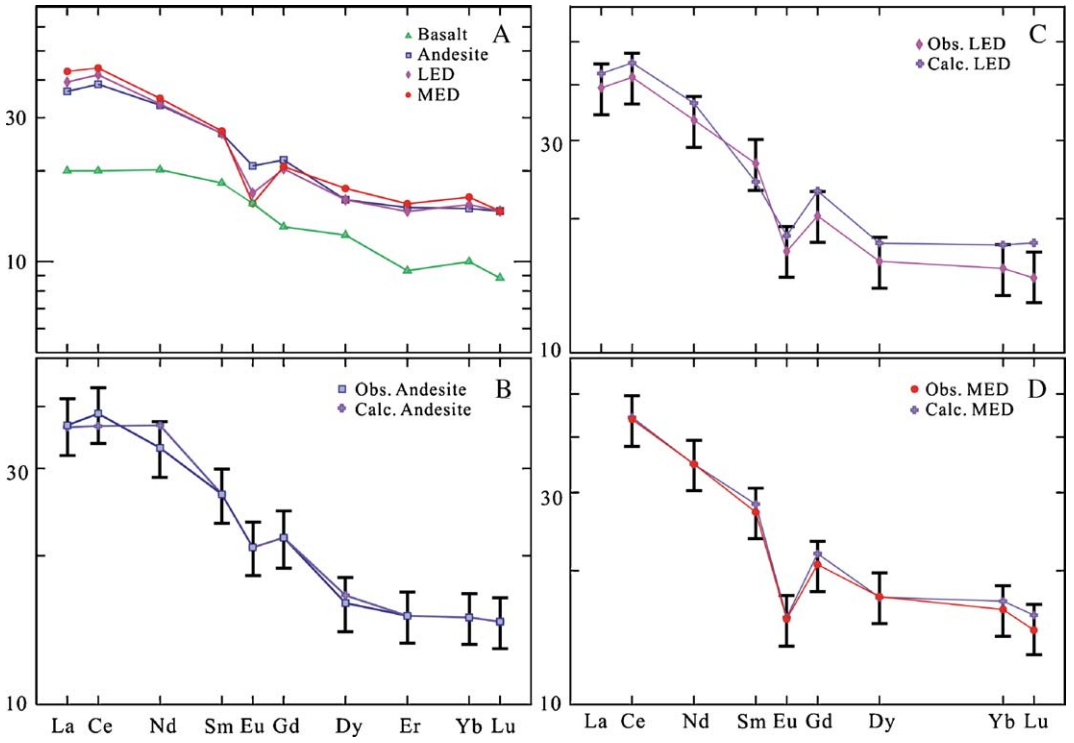

Fig. 4. (A) Chondrite-normalized REE patterns for the Fuji 1707 deposit. (B–D) Chondrite-normalized REE patterns with modeling results. The error bars represent 13% analytical errors based on agreement of standards and linearity of regression lines. Chondrite values are from Nakamura (1974).

mm–2 mm) than does the latter matrix (0.5 mm–0.75 mm). Diktytaxitic texture is observed in some clasts from both matrices.

The andesitic pumices display a variety of colors from white to dark, and some are banded. Phenocryst phases observed in the andesite include plagioclase, hypersthene, augite, magnetite, and apatite. The cores of some plagioclase phenocrysts in the andesite show high anorthite values ($An_{85–90}$), which are comparable to anorthite values in the basalts. The cores of microphenocrysts in the andesite are much more sodic ($An_{59–63}$) than the phenocrysts. Anorthite values in andesite decrease from core to rim, indicating normal zoning. Some plagioclase crystals show disequilibrium textures (Fig. 6A). Olivine gives way to orthopyroxenes which are very distinct with green to light brown pleochroism in more evolved samples (andesite and dacite). Apatite occurs as inclusions within other mineral phases, especially plagioclase (Fig. 6B), observed most commonly in needle shape and less commonly in hexagonal basal cross section. Although light and dark bands are visible in pumices under the microscope, there is no significant change in the mineral phases in different colored bands.

The dacitic pumices display a variety of colors from white to light gray. Some are banded. Phenocryst phases in the dacites are the same as those in the andesite, but are present in smaller percentages. The cores of plagioclase phenocrysts in dacite are much less calcic than those in andesite, ranging

Table 2
Average chemical compositions of phenocrysts. Major elements are in weight percent. Sample indicates the number of samples used to calculate the average chemical compositions. (plg: plagioclase; cpx: clinopyroxene; opx: orthopyroxene; mt: magnetite)

	Basalt		Andesite				Dacite	
	plag	olivine	plag	cpx	opx	mt	plag	opx
Sample	11	4	5	3	1	1	4	3
SiO_2	49.73	38.00	48.92	51.38	52.40	0.78	55.62	52.08
TiO_2	–	–	–	0.41	0.17	9.90	–	0.20
Cr_2O_3	–	0.05	–	0.01	0.07	0.12	–	0.06
Al_2O_3	30.74	–	31.73	1.71	1.49	2.31	27.23	1.54
MgO	–	39.17	–	13.29	23.76	1.85	–	23.47
Fe_2O_3	–	0.00	–	1.07	2.62	48.32	–	2.15
CaO	15.17	0.21	15.55	20.56	1.23	0.07	10.74	1.33
MnO	0.01	0.31	0.01	0.46	0.79	0.45	0.03	0.72
FeO	0.90	23.01	0.91	10.06	18.08	37.47	0.84	18.16
Na_2O	2.61	–	2.44	0.27	–	–	4.00	0.01
K_2O	0.10	–	0.09	–	–	–	0.49	–
NiO	–	0.12	–	–	–	–	–	–
Total	99.26	100.85	99.65	99.23	100.61	101.93	98.95	99.71

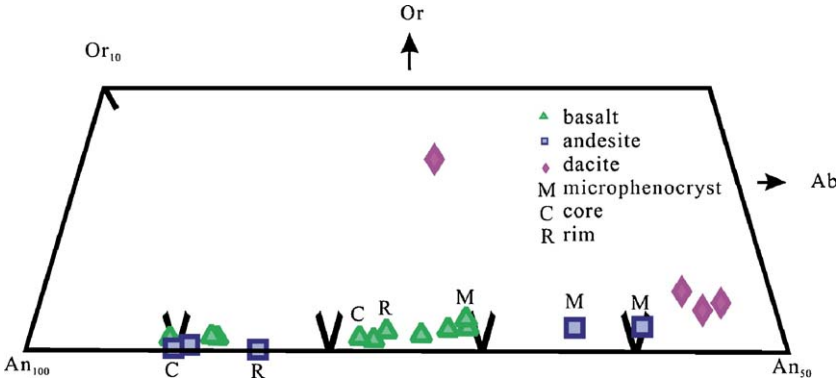

Fig. 5. Feldspar chemical compositions.

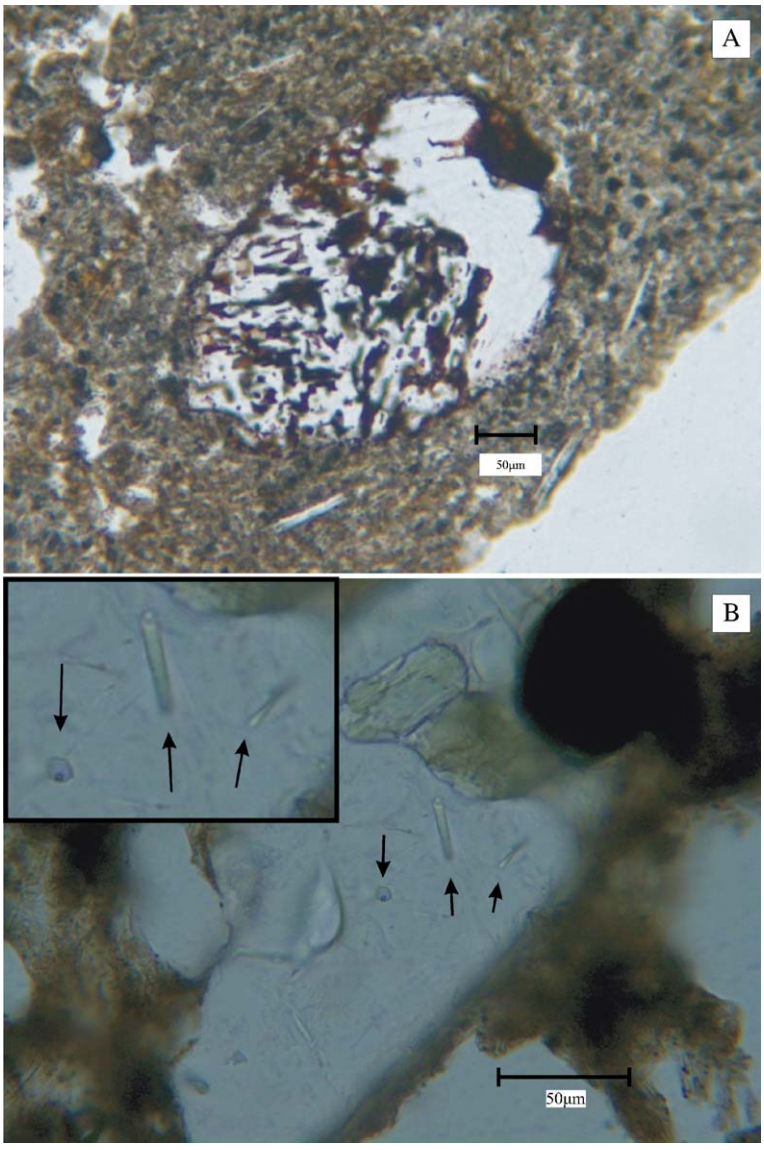

Fig. 6. (A) Petrographic evidence of a disequilibrium texture in a plagioclase crystal in andesite (plane polarized light). (B) Apatite inclusions in plagioclase phenocryst (plane polarized light). The inset is an enlarged view of apatite crystals indicated by arrows.

from $An_{53–69}$. There is no significant difference in chemical compositions of hypersthene and augite from andesite to dacite.

4.3.2. Lithic fragments

The 1707 eruptive products contain a variety of lithic fragments (Tsuya, 1955). Two types of lithic fragments found at the sampling sites are basalts and gabbros. The basalts are gray in color and some are vesicular. They are distinctly denser than the juvenile fragments. The phenocryst assemblage in the basalt fragments is the same as that in the 1707 basalts. The phenocrysts in the basalt fragments are typically euhedral to subhedral and range in diameter from 0.5 mm to 2 mm. The gabbro fragments are very light in color and consist primarily of anorthite (up to 90 vol.%) with very few mafic phases. However, other varieties of gabbros associated with the 1707 eruption have been identified by Yasui et al. (1998), including olivine gabbro norite, gabbro norite, troctolite, and anorthosite. They are thought to be cognate in origin with the Fuji basalts, based on similarities in chemical and mineralogical compositions (Yasui et al., 1998).

4.4. Isotope variations

Sr, Nd, Pb, and Os isotopic compositions of representative juvenile samples and lithic fragments (basalt and gabbro) are summarized in Table 3. All juvenile samples show essentially identical Sr and Nd isotopic signatures with $^{87}Sr/^{86}Sr = 0.70340 \pm 1$ and $^{143}Nd/^{144}Nd = 0.51304 \pm 1$, falling within the typical range for eruptive products from Fuji volcano. All samples also show nearly identical Pb isotopic signatures with $^{206}Pb/^{204}Pb = 18.25 \pm 2$, $^{207}Pb/^{204}Pb = 15.48 \pm 1$, and $^{208}Pb/^{204}Pb = 38.16 \pm 3$. The only Pb isotopic value reported from Fuji Volcano recently is that for JB 3 (Geological Survey of Japan, 2005). JB 3 is a basalt from the 864 AD eruption and is similar to the 1707 samples, with $^{206}Pb/^{204}Pb = 18.27 \pm 2$, $^{207}Pb/^{204}Pb = 15.52 \pm 1$, and $^{208}Pb/^{204}Pb = 38.18 \pm 3$ (Koide and Nakamura, 1990; Matsumoto et al., 1993). All lithic fragment samples show similar Sr, Nd, and Pb isotopic signatures to the juvenile samples.

Os isotopic compositions of the juvenile samples range from $^{187}Os/^{188}Os = 0.165–0.39$. The two basalts show the least radiogenic Os signatures, with $^{187}Os/^{188}Os$ ranging from 0.165 to 0.174 (Fig. 7). These values are slightly elevated compared to mantle-derived basalts from mid-ocean ridges and ocean islands (0.13–0.15; Widom, 1997; Shirey and Walker, 1998) but fall within the range of other arc basalts and sub-arc mantle xenoliths (0.13–0.17; Widom et al., 2003a,b). The more evolved samples (one andesite and two dacites) display radiogenic signatures with $^{187}Os/^{188}Os$ ranging from 0.26 to 0.39.

The Fuji basalts are isotopically distinct from, and generally less radiogenic than most other Japanese island arc basalts (Fig. 8) but are similar to basalts from the Izu-Bonin arc. All samples fall within the Izu-Bonin volcanic front (Izu VF) basalt field on a $^{143}Nd/^{144}Nd$ versus $^{87}Sr/^{86}Sr$ diagram and between overlapping Izu VF and Izu-Bonin back-arc (Izu BA) basalt fields on diagrams of $^{206}Pb/^{204}Pb$ versus $^{87}Sr/^{86}Sr$, $^{207}Pb/^{204}Pb$

Table 3
Sr, Nd, Pb, and Os isotopic compositions and Os concentrations of representative juvenile and lithic fragment samples

	Basalt			Andesite		Dacite	
	JF-10	JF-15	JF-15R	JF-2a	JF-3b	JF-3f	Jf-5c
$^{87}Sr/^{86}Sr$	0.703395	0.703413	–	0.703403	0.703394	0.703406	0.703408
$^{144}Nd/^{143}Nd$	0.513040	0.513043	–	0.513044	0.513043	0.513043	0.513043
$^{206}Pb/^{204}Pb$	18.267	18.268	–	18.252	18.241	18.234	18.225
$^{207}Pb/^{204}Pb$	15.481	15.483	–	15.480	15.472	15.475	15.473
$^{208}Pb/^{204}Pb$	38.185	38.192	–	38.178	38.144	38.145	38.134
$^{187}Os/^{188}Os$	0.174 ± 1	0.165 ± 1	0.171 ± 1	–	0.26 ± 1	0.39 ± 4	0.30 ± 2
Os ppb	0.0024	0.0015	0.0025	–	0.0003	0.0003	0.0003

	Lithic: basalt			Lithic: gabbro		
	JF-6b	JF-6c	JF-8a	JF-7b	Jf-8b	JF-9a
$^{87}Sr/^{86}Sr$	0.703448	0.703368	0.703400	0.703383	0.703416	0.703400
$^{144}Nd/^{143}Nd$	0.513038	0.513047	0.513043	0.513042	0.513040	0.513045
$^{206}Pb/^{204}Pb$	18.261	18.247	–	–	–	–
$^{207}Pb/^{204}Pb$	15.490	15.483	–	–	–	–
$^{208}Pb/^{204}Pb$	38.205	38.158	–	–	–	–

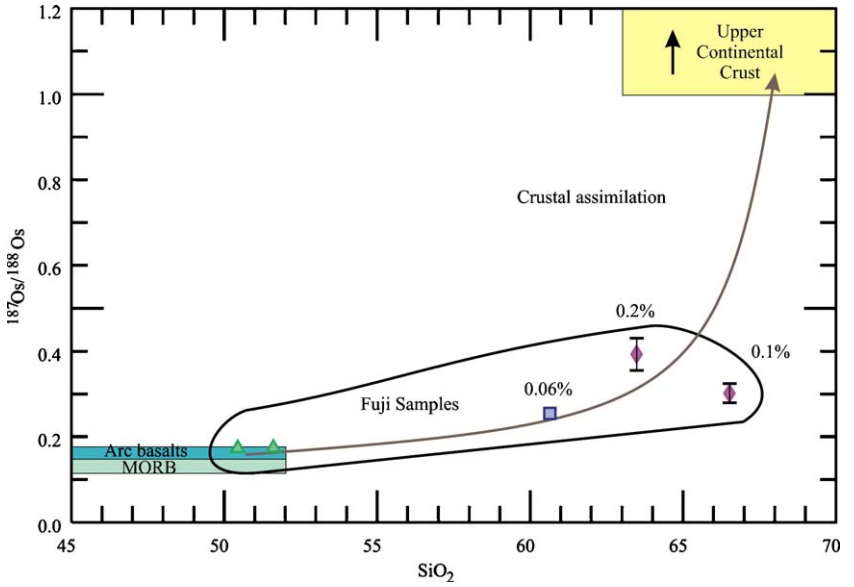

Fig. 7. Os isotopic compositions of representative samples from the Fuji 1707 deposit. Also shown are fields for MORB (Widom, 1997; Shirey and Walker, 1998), arc basalts (Widom et al. 2003a,b), and upper crust (Peucker-Ehrenbrink and Jahn 2001). Labels on data points indicate percentage of crustal assimilation required to produce the observed radiogenic signatures assuming the uncontaminated magmas had 0.3 ppt Os and $^{187}Os/^{188}Os = 0.170$, and the crustal assimilant had 50 ppt Os and $^{187}Os/^{188}Os = 1.06$, similar to estimates for average upper continental crust (Esser and Turekian 1993; Peucker-Ehrenbrink and Jahn 2001). The symbols for basalt, andesite, and dacite are explained in Fig. 2.

and $^{208}Pb/^{204}Pb$ (Fig. 8B–D). The Fuji samples show slightly less radiogenic Pb signatures compared to the Izu VF field but fall within the Izu BA field.

5. Discussion

5.1. Major and trace element variations

Major and trace elements show substantial variations throughout the deposit (Figs. 2, 3). SiO_2 ranges from 50 to 67 wt.%, and other major elements vary accordingly. Most of the trace elements show >3-fold variations, although Zn, Zr, and Ba display <3-fold variations.

A decrease in TiO_2, Al_2O_3, Fe_2O_3, MnO, MgO, CaO, and P_2O_5 with increasing SiO_2 is consistent with fractional crystallization (Fig. 9). Trace element variation diagrams show non-linear trends over the range in SiO_2, indicating changes in fractionating mineral assemblage (Fig. 10). These non-linear trends argue against magma mixing as a dominant process in generating the zonation in the 1707 magma chamber. Furthermore, the Eu abundance of the andesite does not fall between those of basalt and dacite, indicating that andesite was not formed by mixing of basalt and dacite (Fig. 4A).

Least squares major element modeling was done using Igpet 2000 (Carr, 2000). The whole-rock and mineral chemistry used in the major element modeling are summarized in Tables 1 and 2, respectively. The chemical composition for apatite used in the major element modeling was based on average values of 475 samples from apatite in felsic–intermediate rocks not associated with ore deposits (F-NA OD; Piccoli and Candela, 2002). Closed-system fractional crystallization was modeled in three steps, in accordance with observed changes in mineral chemistry and apparent changes in fractionating mineral assemblages suggested by the element–element variation diagrams (Figs. 9, 10), from basalt to andesite, andesite to dacite, and least evolved to most evolved dacite. The results of the major element modeling (summarized in Table 4 and Fig. 9) are consistent with the most evolved dacite forming from a parental magma compositionally similar to the 1707 basalts via ~90% crystallization of a mineral assemblage including plagioclase>hypersthene>augite>magnetite>olivine>apatite. The high degree of fit between observed and modeled liquid compositions are indicated by the low sum of squares of residual (0.07, 0.31, and 0.07; Table 4) for the three modeled fractionation steps, respectively. The major element modeling results are consistent with the observed mineral assemblages, as described previously.

The relative mineral proportions and percentages of crystal fractionation obtained from the major element modeling were applied to trace element modeling (Table 5). The mineral–liquid Kd values were taken from Wil-

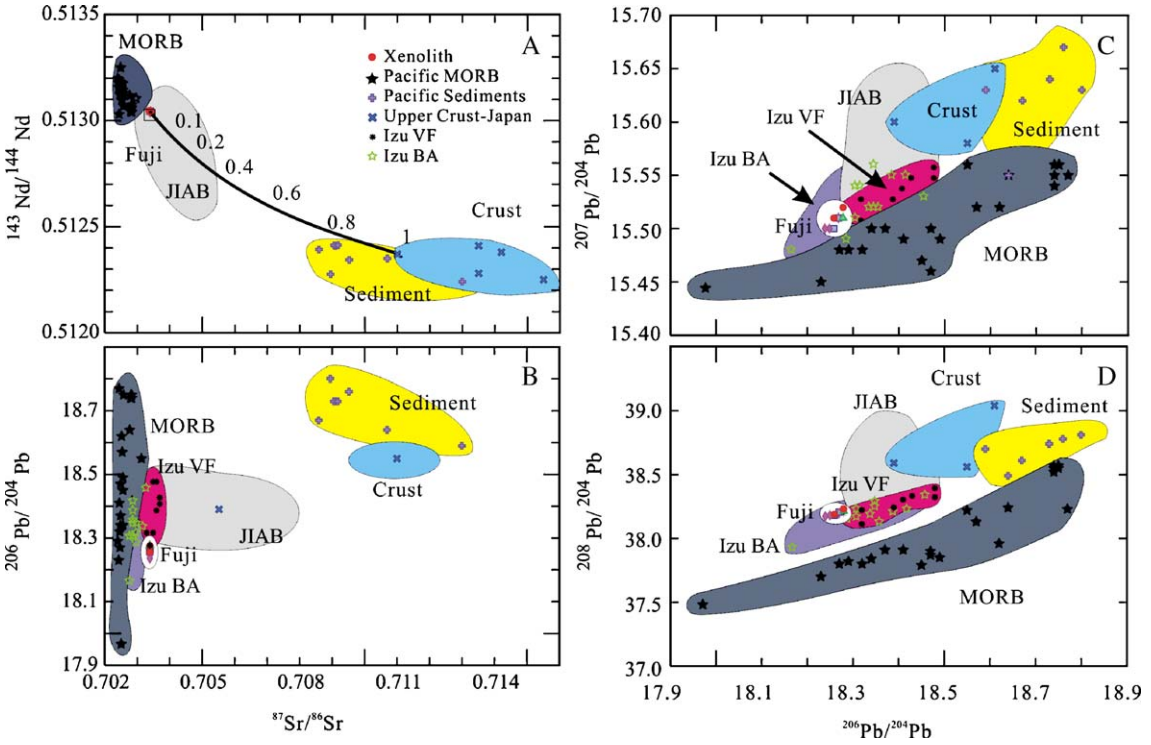

Fig. 8. (A–D) Sr, Nd, and Pb isotopic compositions of juvenile (square in A, white field in B–D) and lithic samples (red circles) from the 1707 deposit. Also shown are fields for Pacific MORB (Ito et al., 1987), Pacific sediments (BenOthman et al., 1989), Japanese upper crust (Geological Survey of Japan, 2005; Rezanov et al., 1999; Kondo et al., 2000), Izu-Bonin volcanic front basalts (Taylor and Nesbitt, 1998), Izu-Bonin back-arc basalts (Hochstaedter et al., 2001), and other Japanese island arc basalts (JIAB, Geological Survey of Japan; Honda and Wasserburg, 1981; Ishizuka and Carlson, 1983; Kimura et al., 1999; Hoang and Uto, 2003). The JIAB field includes Northeast Honshu and Southwest Honshu arc basalts. The square field ($^{143}Nd/^{144}Nd$ vs. $^{87}Sr/^{86}Sr$ diagram) includes all volcanic products from Fuji volcano (Togashi, 1990). The mixing curve shown on the $^{143}Nd/^{144}Nd$ vs. $^{87}Sr/^{86}Sr$ diagram represents bulk mixing between juvenile basalts and typical Japanese upper crust. The end members used for bulk mixing calculation are average basalt and Japanese upper crust (Geological Survey of Japan). Basalt: 389 ppm Sr, $^{87}Sr/^{86}Sr=0.70340$, 12.7 ppm Nd, and $^{143}Nd/^{144}Nd=0.51304$; Japanese upper crust (JG-1, granodiorite): 182 ppm Sr, $^{87}Sr/^{86}Sr=0.7110$, 20.4 ppm Nd, and $^{143}Nd/^{144}Nd=0.51237$. Tick marks on mixing curve represent the fraction of crust assimilated. The symbols for basalt, andesite, and dacite are explained in Fig. 2. For interpretation of the reference to colour in this figure legend, the reader is referred to the web version of this article.

son (1989) and the GERM website (2005). The trace element modeling results are consistent with the major element modeling, with variations in trace element concentrations consistent with changing bulk *D* values for each fractionation step. Sr behaves compatibly, and as fractionation proceeds, the bulk *D* values of Sr change from 1.0 to 1.6 to 2.0 (Fig. 10A). Ba and Zr are both incompatible elements, increasing with increasing SiO_2 (Fig. 10B and C). Bulk *D* values of Ba change from 0.2 to 0.5 to 0.6, while bulk *D* values of Zr change from 0.04 to 0.6 to 0.8 as fractionation proceeds. The modeling results also are consistent with observed REE variations (Fig. 4B–D). All models reproduce observed liquid compositions within analytical error, further indicating the consistency of the major and trace element modeling. These results suggest that crystal fractionation played a major role in the development of chemical zonation in the Fuji 1707 magma chamber.

Geochemical evidence for formation of evolved magmas via extensive fractional crystallization, despite low phenocryst contents in the erupted tephra, is typical of many silicic zoned deposits (e.g., the Bishop, Bandelier, Laacher See, and Fogo A tuffs; Hildreth, 1981, Wolff et al., 1990). Although the physical mechanisms of crystal–liquid separation are beyond the scope of this paper, we note that melt extraction from a mush zone via filter pressing or solidification front compaction or instability (Marsh, 2000; Bachmann and Gergantz, 2004) could explain the formation of a small volume of evolved (andesitic) magma in a largely basaltic system, with a distinct compositional gap, as observed in the Fuji 1707 AD deposit. Subsequent crystal settling and/or sidewall crystallization could contribute to the monotonic chemical gradients within the evolved (andesitic–dacitic) magma, although the importance of these processes is controversial (Bachmann and Ger-

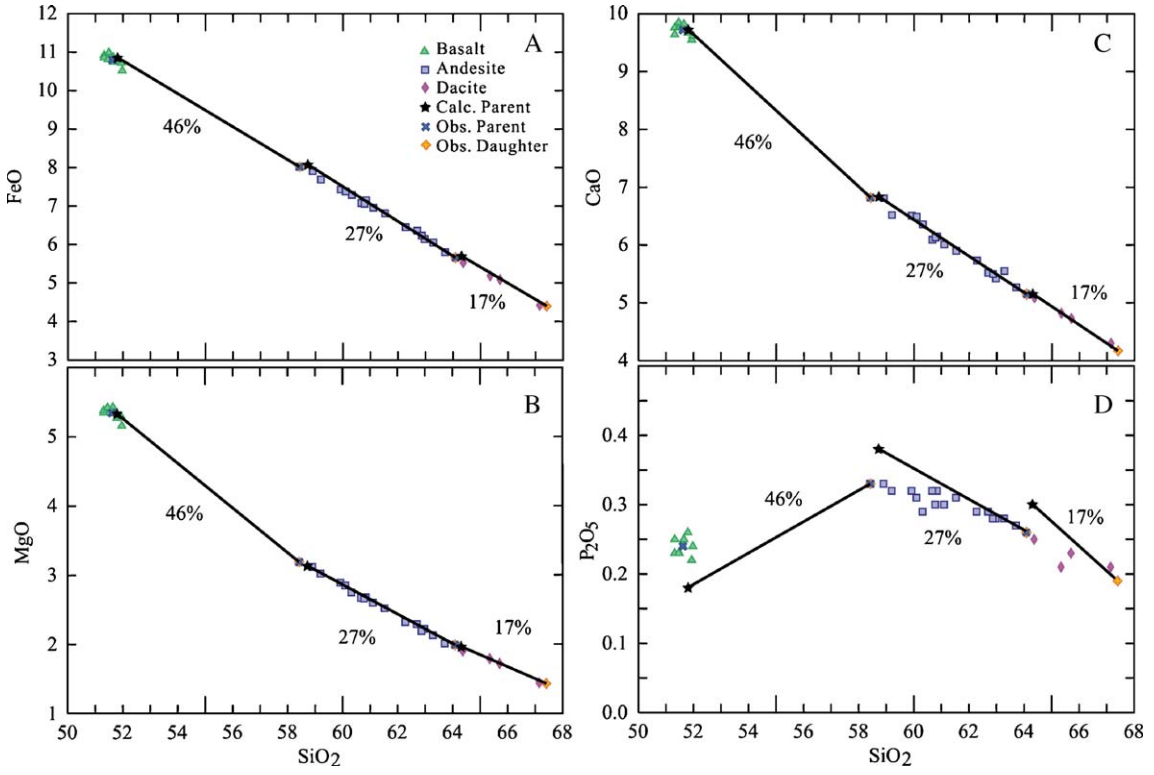

Fig. 9. (A–D) Major element variation diagrams with modeling results. Solid lines indicate modeled trends.

gantz, 2004) and other more complex mechanisms have recently been proposed including convective solidification (Spera et al., 1995) and sinking of solid–liquid mixtures from the crystallization front at the magma chamber roof (Bachmann and Gergantz, 2004).

5.2. Sr–Nd–Pb isotope systematics

All juvenile and lithic samples show essentially identical Sr and Nd isotopic signatures, falling within the typical range for eruptive products from Fuji volcano (Togashi, 1990). All samples also show essentially identical Pb isotopic signatures, similar to the Fuji 864 AD basalt. The lack of variation in the measured isotope ratios from basalts through andesites and dacites indicates that crustal assimilation has not significantly affected the isotope signatures of the Fuji samples, and that the isotopic signatures reflect those of the mantle source beneath Fuji. The Fuji basalts are less radiogenic than other Japanese island arc basalts (Fig. 8), but are similar in Sr, Nd and Pb isotopic signatures to basalts from the Izu-Bonin arc, especially those behind the arc front (Fig. 8).

The significant differences between Fuji and other Japanese island arc basalts indicate either that the mantle beneath Fuji has been less strongly influenced by subduction-related slab fluids or that the Fuji magmas have been less affected by crustal assimilation than other Japanese basalts, or both. The location of Fuji volcano near the trench–trench–trench triple junction (ca. 34°N, 142°E; Aramaki and Ui, 1982) may limit the influx of slab-derived fluids into the mantle wedge in this region. It has been proposed, based on strain partitioning modeling, that a slab tear in the Philippine Sea plate propagates southward beneath Fuji volcano (Mazzotti et al., 1999). This slab tear creates a potential passage for asthenospheric flow (Thorkelson, 1996), which may dilute any influence of slab-derived fluids on the mantle source beneath Fuji compared to other Japanese volcanoes.

5.3. Evidence for open-system behavior

Although closed-system crystal fractionation can explain the observed major and trace element variations and Sr–Nd–Pb isotope signatures, Os isotopes are generally much more sensitive to crustal assimilation due to the extreme difference in $^{187}Os/^{188}Os$ between mantle and crust (Widom and Shirey, 1996; Shirey and Walker, 1998; Widom et al., 1999). The $^{187}Os/^{188}Os$ signatures

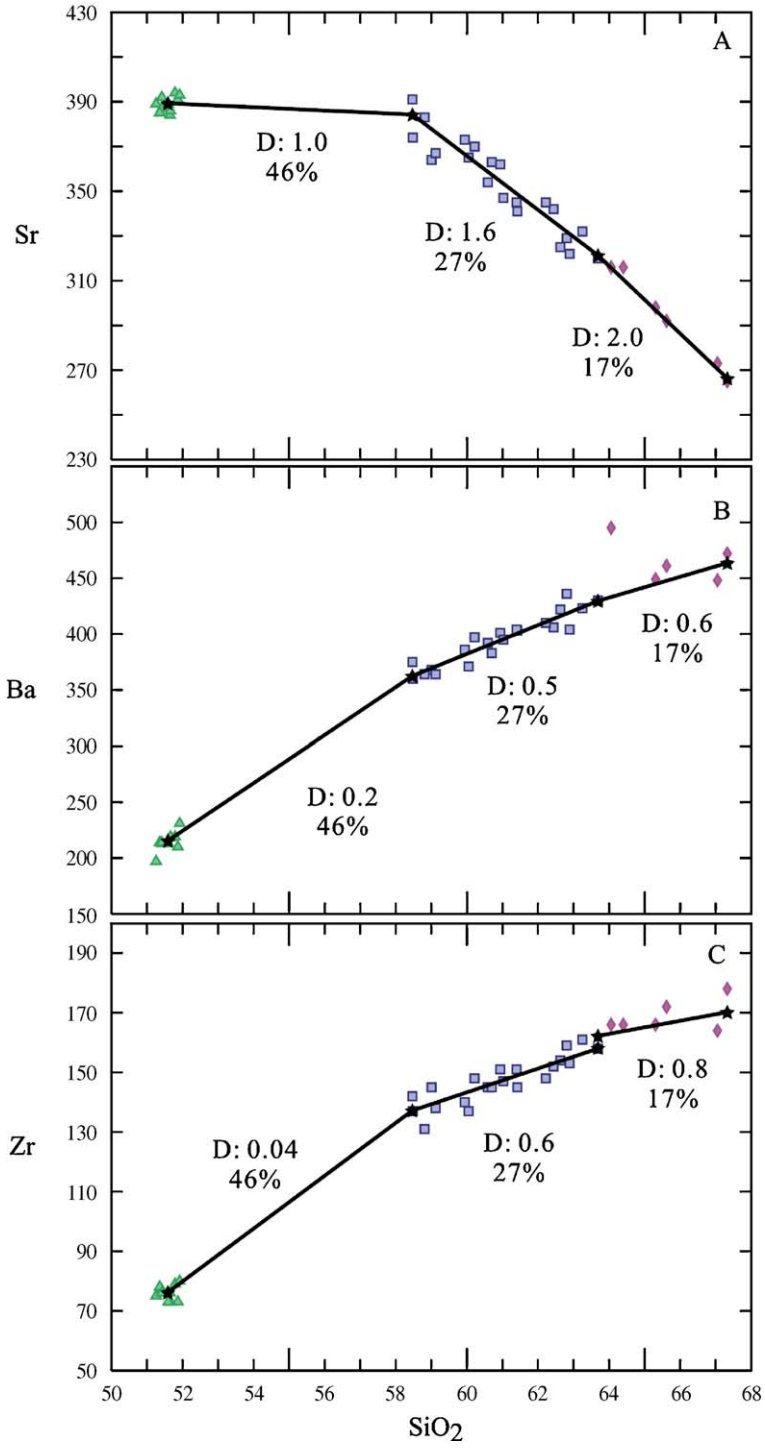

Fig. 10. (A–C) Trace element variation diagrams with modeling results. Stars are the end members used in trace element modeling, while solid lines represent modeled trends. *D* values (*D*) represent partition coefficients (Table 5). The symbols for basalt, andesite, and dacite are explained in Fig. 2.

of the andesite and dacites (0.26–0.39) are distinctly more radiogenic than those of the basalts (0.165–0.174), indicating that crustal assimilation played a role in the formation of the chemically zoned magma chamber. Mixing calculations for assimilation of typical upper crust ($^{187}Os/^{188}Os$ of ~1.0; Peucker-Ehrenbrink and

Table 4
The calculated fractionating mineral assemblages with the relative mineral proportions and the results of major element modeling using Igpet 2000 (Carr, 2000). Major elements are in weight percent. Total Fe as Fe_2O_3 (from DCP-AES) was converted to FeO. (Mineral abbreviations are explained in Table 2; FC%: percentage of fractional crystallization obtained by major element modeling; SSR: sum of squares of residual; obs: observed parent; cal: calculated parent obtained by Igpet from observed daughter.)

	Basalt →		Andesite →		LED →		MED	
%FC		46%		27%		17%		
SSR		0.07		0.31		0.07		
Mineral prop (%)	pl	56%	pl	60%	pl	67%		
	cpx	22%	opx	24%	opx	15%		
	ol	12%	mt	11%	mt	9%		
	mt	10%	cpx	4%	cpx	7%		
			ap	2%	ap	2%		
	Parent obs	calc	Daughter	Parent obs	calc	Daughter	Parent obs	calc	Daughter
SiO_2	51.62	51.81	58.43	58.43	58.72	64.09	64.09	64.31	67.4
TiO_2	1.36	1.13	1.14	1.14	0.92	0.83	0.83	0.75	0.7
Al_2O_3	17.25	17.32	16.88	16.88	16.99	15.94	15.94	16.04	15.42
FeO	10.8	10.85	8.02	8.02	8.07	5.66	5.66	5.69	4.4
MnO	0.19	0.18	0.17	0.17	0.17	0.13	0.13	0.12	0.1
MgO	5.34	5.33	3.19	3.19	3.13	1.99	1.99	1.96	1.43
CaO	9.72	9.72	6.82	6.82	6.83	5.15	5.15	5.15	4.17
Na_2O	2.72	2.66	3.62	3.62	3.18	3.79	3.79	3.58	3.75
K_2O	0.76	0.78	1.4	1.4	1.6	2.16	2.16	2.08	2.44
P_2O_5	0.24	0.18	0.33	0.33	0.38	0.26	0.26	0.30	0.19
NiO	0	0.01	0	0	0	0	0	0	0
Cr_2O_3	0	0.01	0	0	0.01	0	0	0	0
Total	100.00	99.98	100.00	100.00	100.00	100.00	100.00	99.98	100.00

Jahn, 2001) by Fuji magmas indicate that the radiogenic signatures observed in the more evolved Fuji samples could be explained by ≤0.2% of crustal assimilation (Fig. 7), which would not cause significant variation in Sr and Nd isotopes. The basement rocks beneath Fuji (Tertiary marine sediments and green volcanic tuffs; Tsuya, 1955) are likely assimilants, but quantification is not possible due to lack of available chemical and isotopic compositions for these basement rocks. Petrographic features including sieved/resorbed plagioclase crystals (Fig. 6A) can result from crustal contamination due to a change in host liquid composition or incorporation of xenocrysts and may reflect open-system processes that took place prior to the 1707 eruption.

5.4. Proposed model for the evolution of the Fuji 1707 magma chamber

The petrography, major and trace element systematics, and Sr, Nd, Pb, and Os isotope results suggest that the 1707 chemically zoned magma chamber of Fuji Volcano evolved through three main stages, including (1) fractionation of parental magma; (2) formation of an evolved, chemically zoned magma chamber; and (3) basaltic intrusion into the magma chamber. Fig. 11 illustrates each stage as a cartoon diagram.

5.4.1. Stage I: fractionation of parental magma

Because Fuji has erupted almost exclusively basaltic magmas throughout its history, it is inferred that the first stage involved fractional crystallization of basaltic parental magma. The compositional gap between basalt and andesite may indicate that the 1707 basalt is not directly related to the 1707 andesite and dacite. However, it is assumed that the chemical composition of basaltic parental magma that fractionated to form the silicic magmas was similar to the 1707 basalt, based on the chemical similarity of basalts erupted from Fuji Volcano throughout its history (Takahashi et al., 1991). Major, trace, and REE modeling are consistent with 46% crystal fractionation of plagioclase (56%), augite (22%), olivine (12%), and magnetite (10%) from basalt to andesite (Figs. 4B, 9, 10).

5.4.2. Stage II: formation of a chemically zoned magma chamber

During the second stage, fractional crystallization continued within the magma chamber: 27% fractionation of andesite with a crystallizing assemblage of plagioclase (60%), hypersthene (24%), Fe–Ti oxide (11%), augite (4%), and apatite (2%) produced the least evolved dacitic magma (Figs. 4C, 9, 10). Further crystal fractionation formed more evolved dacitic

Table 5
Results of trace element modeling. Bulk D values are calculated using this formula: Bulk $D = \sum Xa*(\mathrm{Kd})a$ where a = mineral phase; X = fraction of mineral in total crystallizing assemblage; and Kd = solid–liquid partition coefficient for the mineral. Kd values are taken from Wilson (1989) and the GERM website (2005; abbreviations are explained in Tables 2 and 4)

Basalt to andesite

Kd	pl	cpx	ol	mt	Bulk D
Zr	0.05	0.003	0.05	0.02	0.04
Ba	0.2	0.05	0.03	0.03	0.2
Sr	1.8	0.06	0.01	0.1	1.0
La	0.02	0.002	0.0004	0.02	0.01
Ce	0.02	0.02	0.007	0.02	0.02
Nd	0.01	0.06	0.005	0.03	0.02
Sm	0.5	0.2	0.03	0.2	0.3
Eu	0.3	1	0.03	0.3	0.4
Gd	0.007	0.6	0.1	0.02	0.2
Dy	0.3	1	0.007	0.3	0.5
Er	0.04	0.5	0.2	0.01	0.2
Yb	0.06	1.1	0.04	0.5	0.3
Lu	0.04	1.1	0.02	0.02	0.3
FC%	56%	22%	12%	10%	100%

Andresite to least evolved dacite (LED)

Kd	pl	opx	cpx	mt	ap	Bulk D
Zr	0.5	0.04	0.8	2.2	0.6	0.6
Ba	0.7	0.02	0.1	0.4	0.05	0.5
Sr	2.5	0.005	0.3	0.1	1.3	1.6
La	0.4	0.03	0.05	0.5	14.5	0.5
Ce	0.2	0.04	0.08	0.4	21.1	0.5
Nd	0.1	0.03	0.2	0.6	32.8	0.7
Sm	0.8	0.05	0.4	0.6	46.0	1.3
Eu	1.3	0.08	3.0	0.5	25.5	1.4
Gd	0.07	0.04	0.6	0.3	43.9	0.8
Dy	0.05	0.08	0.8	0.6	34.8	0.7
Yb	0.06	0.6	1.0	0.5	15.4	0.5
Lu	0.04	0.3	0.7	0.4	13.8	0.4
FC%	60%	24%	4%	11%	2%	100%

Least evolved dacite (LED) to most evolved dacite (MED)

Kd	pl	opx	mt	cpx	ap	Bulk D
Zr	0.6	0.03	3.9	0.2	0.6	0.8
Ba	0.9	0.02	0.03	0.4	0.05	0.6
Sr	2.9	0.1	0.08	0.1	1.3	2.0
Ce	0.3	0.02	0.06	0.04	21.0	0.7
Nd	0.3	0.02	0.6	0.2	26.0	0.8
Sm	0.2	0.02	0.07	0.5	27.0	0.7
Eu	1.5	0.3	0.06	0.4	14.5	1.4
Gd	0.1	0.03	0.3	0.7	21.7	0.6
Dy	0.2	0.04	0.6	0.8	16.9	0.6
Yb	0.3	0.1	0.1	0.6	9.4	0.5
Lu	0.3	0.2	0.1	0.7	16.0	0.6
FC%	67%	15%	9%	7%	2%	100%

magma: 17% fractionation of plagioclase (67%), hypersthene (15%), magnetite (9%), augite (7%), and apatite (2%) can explain the chemical compositions of the most evolved samples from the 1707 deposit (Figs. 4D, 9, 10). During stage II, a very minor amount of crustal assimilation occurred. Minor crustal assimilation is required to explain the elevated $^{187}Os/^{188}Os$ signatures in the more evolved samples. The small amount of assimilation would not be expected to significantly affect the major and trace elements or the Sr, Nd, and Pb isotope signatures.

5.4.3. Stage III: Plinian eruption of dacite and andesite followed by Subplinian to Plinian basaltic eruption

After a chemically zoned magma chamber consisting of andesite and dacite was formed via fractional crystallization accompanied by very minor crustal assimilation, the silicic magmas were violently erupted. Two possible eruption triggering mechanisms include volatile oversaturation via crystal fractionation (Blake, 1984) and basaltic intrusion into a pre-existing silicic magma chamber (Sparks et al, 1977). It has been proposed by Fujii et al. (2003) that basaltic intrusion into a silicic magma pocket caused superheating accompanied by subsequent vesiculation and convection within the magma pocket and triggered the eruption.

Although no large-scale mingling/mixing between basalt and andesite was observed, basaltic magma was most likely intruded into a pre-existing chemically zoned magma chamber as proposed by Fujii et al. (2003). Self-mixing induced by basaltic intrusion into the base of the magma chamber (Couch et al., 2001) may be responsible for some resorbed plagioclase phenocrysts and relatively high anorthite values in the andesites.

5.5. Liquid immiscibility

Although liquid immiscibility is a common small-scale process in basaltic magmas (Philpotts, 1976, 1982; Fujii et al., 1980), it has not been recognized as a magma chamber-scale process in silicic magmas. All major, trace, and REE modeling for the Fuji 1707 deposit are consistent with fractional crystallization as the dominant petrogenetic process. Although Kawamoto (1990, 1991a,b, 1992) suggested that the observed trace element abundances and the decrease in P_2O_5 from andesite to dacite could not be explained by fractional crystallization, our study shows that elemental variations are in fact consistent with fractional crystallization. The fact that fractional crystallization is a common process, and that it can easily explain the observed chemical gradients in the magma chamber, leads us to favor this model. We find that there is no

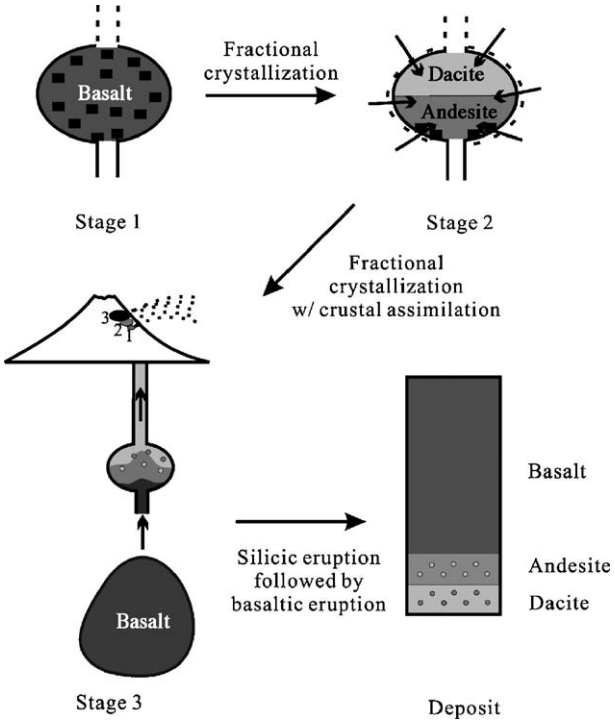

Fig. 11. Cartoon diagram of the evolution of the 1707 chemically zoned magma chamber. Stage 1: fractionation of parental basaltic magma to form evolved magma. Stage 2: formation of a chemically zoned magma chamber by crystal fractionation with minor crustal assimilation. Stage 3: intrusion of basaltic magma into the chamber, triggering Plinian eruption of evolved (andesitic and dacitic) magma followed by a much greater eruptive volume of basaltic magma.

need to resort to unusual processes such as liquid immiscibility to explain the 1707 chemically zoned magma chamber.

6. Conclusions

Major and trace element concentrations show substantial variations throughout the Fuji 1707 deposit. Decreasing abundances of MgO, CaO, Al_2O_3, and P_2O_5 with increasing SiO_2 and non-linear trends on trace element variations are best explained by fractional crystallization of the observed phenocryst assemblage. Trace element models are consistent with the major element modeling. Chondrite-normalized REE abundances show expected enrichment from basalt to andesite and display strong negative Eu anomalies that increase from andesite to dacite, further supporting magma evolution by fractional crystallization. Sr, Nd, and Pb isotopic compositions show essentially identical signatures throughout the deposit. Although these observations are all consistent with closed-system fractional crystallization, a very minor amount of crustal contamination is required by the radiogenic Os isotope signatures in the more evolved samples.

Our combined geochemical, isotopic, and petrographic observations suggest that the 1707 magma chamber evolved through three main stages including (1) fractionation of parental basaltic magma; (2) formation of an evolved chemically zoned magma chamber by fractional crystallization and minor crustal assimilation; and (3) intrusion of basaltic magma into the chamber, triggering Plinian eruption of evolved (andesitic and dacitic) magma followed by a much greater eruptive volume of basaltic magma.

Acknowledgement

The authors thank Dr. Arata Sugimura, Dr. John Morton, Dr. William K. Hart, Dr. John Rakovan, Dave Kuentz, Dr. Darin Snyder, Ninad Bondre, Olaf Borkiewicz, and Dr. Richard Edelmann for their assistance in sample collection and laboratory analyses. We also thank Dr. Bruce Marsh, Dr. John Wolff, and anonymous reviewers for their constructive comments. This research was funded by NSF EAR 020759 and EAR-MRI 0116033 (to EW) and Geological Society of America 7303-02 and Sigma Xi (to SW).

References

Aramaki, S., Ui, T., 1982. Japan. In: Thorpe, R.S. (Ed.), Andesites Orogenic Andesites and Related Rocks. John Wiley and Sons Ltd, Great Britain, p. 724.

Arculus, R.J., Gust, D.A., Kushiro, I., 1991. The evolution of Fuji and Hakone Volcanoes Honshu: research and exploration: a scholarly publication of the National Geographic Society, vol. 7, pp. 276–309.

Bachmann, O., Gergantz, G.W., 2004. On the origin of crystal-poor rhyolites: extracted from batholithic crystal mushes. J. Petrol. 45, 1565–1582.

BenOthman, D.B., White, W.M., Patchett, J., 1989. The geochemistry of marine sediments, island arc magma genesis, and crust–mantle recycling. Earth Planet. Sci. Lett. 94, 1–21.

Blake, S., 1984. Volatile oversaturation during the evolution of silicic magma chambers as an eruption tripper. J. Geophys. Res. 89, 8237–8244.

Brooker, R.A., 1998. The effect of CO_2 saturation on immiscibility between silicate and carbonate liquids: an experimental study. J. Petrol. 39, 1905–1915.

Carr, M., 2000. Igpet 2000 for Win95/98/NT. Terra Softa Inc.

Cohen, A.S., Waters, F.G., 1996. Separation of osmium from geological materials by solvent extraction for analysis by thermal ionisation mass spectrometry. Anal. Chim. Acta 332, 269–275.

Couch, S., Sparks, R.S.J., Carroll, M.R., 2001. Mineral disequilibrium in lavas explained by convective self-mixing in open magma chambers. Nature 411, 1037–1039.

Duffield, W.A., Ruiz, J., Webster, J.C., 1995. Roof-rock contamination of magma along the top of the reservoir for the Bishop Tuff. J. Volcanol. Geotherm. Res. 69, 187–195.

Esser, B.K., Turekian, K.K., 1993. The osmium isotopic composition of the continental crust. Geochim. Cosmochim. Acta 57, 3093–3104.

Fujii, T., Kushiro, I., Nakamura, Y., Koyaguchi, T., 1980. A note on silicate liquid immiscibility in Japanese volcanic rocks. J. Geol. Soc. Japan 86, 409–412.

Fujii, T., Yoshimoto, M., Kaneko, T., Nakada, S., Yasuda, A., 2003. Ejecta of Fuji 1707 eruption: compositional variation and eruption sequence. Geol. Soc. Japan Abs, 26.

Geological Survey of Japan, 2005. http://www.aist.go.jp/RIODB/geostand/welcome.html.

GERM, 2005. http://earthref.org/GERM/tools/petrology.

Hildreth, W., 1981. Gradients in silicic magma chambers: implications for lithospheric magmatism. J. Geophys. Res. 86, 10153–10192.

Hoang, N., Uto, K., 2003. Ceochemistry of Cenozoic basalts in the Fukuoka district (northern Kyushu, Japan): implications for asthenosphere and lithospheric mantle interaction. Chem. Geol. 198, 249–268.

Hochstaedter, A., Gill, J., Peters, R., Broughton, P., Holden, P., Taylor, B., 2001. Across-arc geochemical trends in the Izu-Bonin arc: contributions from the subducting slab. Geochem. Geophys. Geosyst. 2 2000GC000105.

Honda, S., Wasserburg, G.J., 1981. Nd and Sr isotopic study of volcanic rocks from Japan. Earth Planet. Sci. Lett. 52, 264–276.

Ishizuka, K., Carlson, R.W., 1983. Nd–Sr systematics of the Setouchi volcanic rocks, southwest Japan: a clue to the origin of orogenic andesite. Earth Planet. Sci. Lett. 64, 327–340.

Ito, E., White, W.M., Gopel, C., 1987. The O, Sr, Nd and Pb isotope geochemistry of MORB. Chem. Geol. 62, 157–176.

Katoh, S., Danhara, T., Hart, W.K., Gabriel, G.W., 1999. Use of sodium polytungstate solution in the purification of volcanic glass shards for bulk chemical analysis. Nat. Hum. Activ. 4, 45–54.

Kawamoto, T., 1990. Liquid immiscibility in a calc-alkaline magma chamber, the Hoei Tephra, Fuji Volcano, Japan. AGU Abs 31, 952.

Kawamoto, T., 1991a. Liquid immiscibility in the Fuji 1707 calc-alkaline magma chamber, Japan. AGU Abs 52, 575.

Kawamoto, T., 1991b. Mechanism for the formation of the Fuji 1707 magma chamber, Japan: liquid immiscibility in calc-alkaline magmas. Volcanol. Soc. Japan Abs, 169.

Kawamoto, T., 1992. Liquid immiscibility in the Fuji 1707 calc-alkaline magma chamber, Japan. IGC Abs 29, 558.

Kimura, J., Manton, W.I., Sun, C., Iizumi, S., Yoshida, T., Stern, R.J., 1999. Chemical diversity of the Ueno Basalts central Japan: identification of mantle and crust contributions to arc basalt. AGU Abs, 1203.

Koide, Y., Nakamura, E., 1990. Lead isotope analyses of standard rock samples. Mass Spectrosc. 38, 241–251.

Kondo, H., Shuto, K., Fukase, M., 2000. An AFC (assimilation and fractional crystallization) process as the petrogenesis of andesites from the Pliocene Myojin-iwa Formation, the back-arc side of the Northeast Japan: combined major- and trace-element and Sr–Nd isotope constraints. J. Geol. Soc. Japan 106, 426–441.

Koyama, M., 1998. Reevalution of the eruptive history of Fuji Volcano, Japan, mainly based on historical documents. Bull. Volcanol. Soc. Japan 43, 323–347.

Koyama, M., Nishiyama, A., Sumiya, H., Inoue, K., Sasahara, K., Anyoji, N., 2002. Reconstruction of the 1707 Hoei eruption of Fuji Volcano, Japan, based on historical documents. Earth Planet. Sci. Japan Abs, 25.

LeBas, M.J., LeMaitre, R.W., Streckeisen, A., Zanettin, B.A., 1986. Chemical classification of volcanic rocks based on the total alkali–silica diagram. J. Petrol. 27, 745–750.

Machida, H., 1964. Tephrochronological study of Volcano Fuji and adjacent areas. J. Geogr. Japan (Chigaku-zasshi) 73 (293–308), 337–350.

Marsh, B.D., 2000. Magma chambers. In: Sigurdsson, H., Houghton, B., McNutt, S.R., Rymer, H., Stix, J. (Eds.), Encyclopedia of volcanoes. Academic Press, San Diego, CA, pp. 191–206.

Matsumoto, A., Hirao, Y., Togashi, S., 1993. Determination of lead isotope ratio of GSJ rock reference samples. Bull. Geol. Surv. Japan 44, 649–657.

Mazzotti, S., Henry, P., LePichon, X., Sagiya, T., 1999. Strain partitioning in the zone of transition from Nankai subduction to Izu-Bonin collision (Central Japan): implications for an extensional tear within the subducting slab. Earth Planet. Sci. Lett. 172, 1–10.

Michael, P.J., 1983. Chemical differentiation of the Bishop Tuff and other high-silica magmas through crystallization processes. Geology 11, 31–34.

Miyaji, N., 1984. Wind effect on the dispersion of the Fuji 1707 tephra. Bull. Volcanol. Soc. Japan 29, 17–30.

Miyaji, N., 1988. History of Younger Fuji Volcano. J. Geol. Soc. Japan 94, 433–452.

Nakamura, N., 1974. Determination of REE, Ba, Fe, Mg, Na and K in carbonaceous and ordinary chondrites. Geochim. Cosmochim. Acta 38, 757–775.

Nier, A.O., 1950. A redetermination of the relative abundances of the isotopes of carbon, nitrogen, oxygen, argon and potassium. Phys. Rev. 77, 789–793.

Peucker-Ehrenbrink, B., Jahn, B., 2001. Rhenium–osmium isotope systematics and platinum group element concentrations: loess and the upper continental crust. Geochem. Geophys. Geosyst. 2 2001GC000172.

Philpotts, A.R., 1976. Silicate liquid immiscibility: its probable extent and petrogenetic significance. Am. J. Sci. 276, 1147–1177.
Philpotts, A.R., 1982. Compositions of immiscible liquids in volcanic rocks. Contrib. Mineral. Petrol. 80, 201–218.
Piccoli, P.M., Candela, P.A., 2002. Apatite in igneous system. In: Kohn, M.J., Rakovan, J., Hughes, J.M.Reviews in Mineralogy and Geochemistry, vol. 48. Mineral Soc. America, Washington, DC, pp. 225–292.
Pin, C., Zalduegui, J.F.S., 1997. Sequential separation of light rare-earth elements, thorium and uranium by miniaturized extraction chromatography: application to isotopic analyses of silicate rocks. Anal. Chim. Acta 339, 79–89.
Rezanov, A.I., Shuto, K., Iizumi, S., Shimura, T., 1999. Sr and Nd isotopic and geochemical characteristics of Cretaceous Paleogene granitoid rocks in the Niigata area, the northernmost part of the Southwest Japan. Mem. Geol. Soc. Japan 53, 269–297.
Roy-Barman, M., 1993. Mesure du rapport $^{187}Os/^{186}Os$ dans les basalts et peridotites: contribution a la systematique $^{187}Re/^{186}Os$ dans le manteau, Thesis, Univ. Paris 7.
Roy-Barman, M., Allegre, C.J., 1995. $^{187}Os/^{186}Os$ in ocean island basalts: tracing oceanic crust recycling in the mantle. Earth Planet. Sci. Lett. 129, 145–161.
Shirey, S.B., Walker, R.J., 1995. Carius tube digestion for low-blank rhenium–osmium analysis. Anal. Chem. 34, 2136–2141.
Shirey, S.B., Walker, R.J., 1998. The Re–Os isotope system in cosmochemistry and high-temperature geochemistry. Annu. Rev. Earth Planet. Sci. 26, 423–500.
Snyder, D.C., 2005. Processes and Time Scales of Differentiation in Silicic Magma Chambers: Chemical and Isotopic Investigations. PhD dissertation, Miami University, 227p.
Snyder, D.C., Widom, E., Pietruszka, A.J., Carlson, R.W., 2004. The role of open-system processes in the development of silicic magma chambers: a chemical and isotopic investigation of the Fogo A trachyte deposit, São Miguel, Azores. J. Petrol. 45, 723–738.
Sparks, S.R.J., Sigurdsson, H., Wilson, L., 1977. Magma mixing: a mechanism for triggering acid explosive eruptions. Nature 267, 315–318.
Spera, F.J., Oldenburg, C.M., Christensen, C., Todesco, M., 1995. Simulations of convection with crystallization in the system $KAlSi_2O_6$–$CaMgSi_2O_6$: implication for compositionally zoned magma bodies. Am. Mineral. 80, 1188–1207.
Taira, A., 2001. Tectonic evolution of the Japanese island arc system. Annu. Rev. Earth Planet. Sci. 29, 109–134.
Takahashi, M., Hasegawa, Y., Tsukui, M., Nemoto, Y., 1991. Evolution of magma-plumbing system beneath Fuji Volcano: on the viewpoint of whole-rock chemistry. Bull. Volcanol. Soc. Japan 36, 281–296.
Taylor, R.N., Nesbitt, R.W., 1998. Isotopic characteristics of subduction fluids in an intra-oceanic setting, Izu-Bonin Arc, Japan. Earth Planet. Sci. Lett. 164, 79–98.
Thorkelson, D.J., 1996. Subduction of diverging plates and the principles of slab window formation. Tectonophysics 255, 47–63.
Todt, W., Cliff, R.A., Hanser, A., Hofmann, A.W., 1996. Evaluation of a ^{202}Pb–^{205}Pb double spike for high precision lead isotope analysis. In: Basu, A., Hart, S. (Eds.), Earth Processes: Reading the Isotopic Code, AGU Mongraph, vol. 95, pp. 429–437.
Togashi, S., 1990. Geochemical history of Fuji Volcano and constraint on the model of magma chamber. Volcanol. Soc. Japan Abs 1, 10.
Tsuya, H., 1940. Geological and petrological studies of Volcano Fuji III: geology of the southwestern foot of Volcano Fuji. Bull. Earthq. Res. Inst. 18, 419–445.
Tsuya, H., 1955. Geological and petrological studies of Volcano Fuji V: on the 1707 eruption of Volcano Fuji. Bull. Earth. Res. Inst. 33, 341–383.
Walker, R.J., Carlson, R.W., Shirey, S.B., Boyd, S.B., 1989. Os, Sr, Nd and Pb isotope systematics of southern African peridotite xenoliths: implications for the chemical evolution of subcontinental mantle. Geochim. Cosmochim. Acta 53, 1583–1595.
Widom, E., 1997. Sources of ocean island basalts: a review of the osmium isotope evidence. Physica A 244, 484–496.
Widom, E., Shirey, S.B., 1996. Os isotope systematics in the Azores: implications for mantle plume sources. Earth Planet. Sci. Lett. 142, 451–465.
Widom, E., Gill, J.B., Schmincke, H.U., 1992. Processes and time-scales in the evolution of chemically zoned trachyte; Fogo A, Sao Miguel, Azores. Contrib. Mineral. Petrol. 111, 311–328.
Widom, E., Hoernle, K.A., Shirey, S.B., Schmincke, H.U., 1999. Os isotope systematics in the Canary Islands and Madeira: lithospheric contamination and mantle plume signatures. J. Petrol. 40, 279–296.
Widom, E., Kepezhinskas, P., Defant, M., 2003a. The nature of metasomatism in the sub-arc mantle wedge: evidence from Re–Os isotopes in Kamchatka peridotite xenoliths. Chem. Geol. 196, 283–306.
Widom, E., Kepezhinskas, P., Defant, M., 2003b. Os and Sr isotope signatures in Kamchatka Adakites, Nb-rich arc basalts and mantle pyroxenites: inferences on mantle and crustal processes. EOS Abst vol. San Francisco.
Wilson, M., 1989. Igneous Petrogenesis: a Global Tectonic Approach. Unwin Hyman Ltd, London.
Wolff, J.A., Ramos, F.C., 2003. Pb isotope variations among Bandelier Tuff feldspars: no evidence for a long-lived silicic magma chamber. Geology 31, 533–536.
Wolff, J.A., Worner, G., Blake, S., 1990. Gradients in physical parameters in zoned felsic magma bodies: implications for evolution and eruptive withdrawal. J. Volcanol. Geotherm. Res. 43, 37–55.
Wörner, G., Schmincke, H.U., 1984. Mineralogical and chemical zonation of the Laacher See Tephra Sequence (East Eifel, W. Germany). J. Petrol. 25, 805–835.
Wörner, G., Wright, T.L., 1984. Evidence for magma mixing within the Laacher See magma chamber (East Eifel, Germany). J. Volcanol. Geotherm. Res. 22, 301–327.
Yasui, M., Togashi, S., Shimomura, Y., Sakamoto, S., Miyaji, N., Endo, K., 1998. Petrological features and origin of the gabbroic fragments contained in the 1707 pyroclastic fall deposits, Fuji Volcano. Bull. Volc. Soc. Japan 43, 43–59.